Journal of the European Ceramic Society 39 (2019) 2446–2452

Contents lists available at ScienceDirect

Journal of the European Ceramic Society

journal homepage: www.elsevier.com/locate/jeurceramsoc

Original article

Application of Judd–Ofelt theory in analyzing Nd^{3+} doped SrF_2 and CaF_2 transparent ceramics

Zhiwei Zhou[a], Weiwei Li[a], Jinghong Song[b], Bingchu Mei[a,*], Guoqiang Yi[a], Yu Yang[a]

[a] State Key Laboratory of Advanced Technology for Materials Synthesis and Processing, Wuhan University of Technology, Wuhan, 430070, China
[b] Center of Materials Research and Analysis, Wuhan University of Technology, Wuhan, 430070, China

ARTICLE INFO

Keywords:
Judd-Ofelt theory
Nd^{3+}
SrF_2
CaF_2
Transparent ceramics

ABSTRACT

Nd^{3+} doped SrF_2 and CaF_2 transparent ceramics were fabricated by vacuum hot-press sintering and the absorption spectra, emission spectra as well as luminescence decays of the samples were measured. Judd-Ofelt (J–O) theory was used to analyze the optical performance of Nd^{3+} in these two isostructural hosts. The Nd: SrF_2 transparent ceramic was found to have smaller line strength, larger radiative lifetime and smaller Ω_2 value (corresponding to more ionic Nd^{3+}-ligand bonding and more symmetry of Nd^{3+} environment). These features made it easier for Nd: SrF_2 to realize population inversion and strong emission, thus doing good to laser performance. The strong emission of $^4F_{3/2} \rightarrow {}^4I_{9/2}$ transition in Nd: SrF_2, which was predicted by J–O theory and demonstrated by luminescence spectrum, made it possible to achieve effective laser output around 900 nm. The intensity parameters and radiative lifetimes of ceramics were found comparable with their corresponding single crystals.

1. Introduction

RE^{3+} doped alkaline-earth fluoride single crystals and transparent ceramics are served as promising materials for various optical applications and therefore, they are vastly investigated [1–5]. Among them, Nd^{3+} doped SrF_2 and CaF_2 single crystals raised increasing attention in the past decade [6–8] for they were highly expected for the development of solid-state lasers and laser amplifiers. Generally, compared with single crystals, the transparent ceramic hosts provide better physical properties such as higher mechanical strength and fracture toughness [9], higher RE^{3+} active ions concentration capacity, larger size and easier acquisition [10]. Therefore, plenty of works had transferred to the fabrication of highly optical quality transparent ceramics. For example, Lyberis and co-workers successfully fabricated Yb: CaF_2 transparent ceramic with laser action by hot-pressing the nano-sized powder [11]. Basiev and his team reported an application of hot-forming technique in preparing SrF_2 and CaF_2 laser ceramics from single crystals [12–14]. However, as for optical properties, except for that the single crystals provide higher transmittance than ceramics, the understanding of other optical properties between SrF_2/CaF_2 single crystals and their corresponding transparent ceramics still remains uncertain since very few literatures are available on the comparison between these materials.

The UV-VIS-NIR absorption spectra based Judd-Ofelt theory [15,16] was widely used as a fundamental tool in analyzing 4f → 4f inner shell electronic transitions [17–21]. This is because many essential optical parameters, such as intensity parameters Ω_t (t = 2, 4, 6), line strengths, radiative lifetimes, branching ratios and transition rates, can be calculated from J–O theory, thus offering possibility to characterize and evaluate the optical properties of RE^{3+} doped materials. For instance, Mehta et al. [17] draw a conclusion that multiphonon non-radiative relaxation processes occurred in the Nd^{3+} doped phosphate and borate glasses because the measured fluorescence lifetimes were much shorter than the radiative lifetimes calculated from J–O theory. Karunakaran et al. [18] reported that because of smaller spectroscopic quality factors (Ω_4/Ω_6), the $^4F_{3/2} \rightarrow {}^4I_{11/2}$ laser emissions in Nd^{3+} doped fluoroborate glasses were relatively intense. Wang et al. [19] examined the optical features of Nd^{3+} doped CaF_2 crystal in the frame work of J–O theory.

Based on these introductions, it is certainly that the applications of J–O theory in RE^{3+} doped SrF_2 and CaF_2 transparent ceramics are of prominent importance, particularly these materials are attracting growing interests in recent years [22–27]. However, to our best knowledge, the existing literatures available on RE^{3+} doped SrF_2 and CaF_2 transparent ceramics are mostly focused on the study of their synthesis and microstructure, although some of the literatures have studied their optical properties, but none of them is related to J–O theory. On the other hand, despite of so many studies on RE^{3+} doped CaF_2 transparent ceramics were published, the reports on RE^{3+} doped

* Corresponding author at: 122 Luoshi Road, Wuhan, Hubei, China.
E-mail address: bcmeilab@163.com (B. Mei).

https://doi.org/10.1016/j.jeurceramsoc.2019.02.033
Received 24 October 2018; Received in revised form 6 February 2019; Accepted 15 February 2019
Available online 16 February 2019
0955-2219/

SrF_2 were rather sparsely, let alone reports on comparison between these two isostructural transparent ceramics. Motivated by this, we used the J–O theory to investigate the optical properties of Nd^{3+} doped SrF_2 and CaF_2 transparent ceramics for the first time in this work. The first goal of this work is the applications of J–O theory in Nd^{3+} doped SrF_2 and CaF_2 transparent ceramics, namely, is to figure out the optical parameters of Nd^{3+} in these two isostructural ceramic hosts. The next to be done is to evaluate and compare the optical performance between Nd: SrF_2 and Nd: CaF_2 transparent ceramics from a basis of the obtained optical parameters. To have a better understanding of optical properties between SrF_2/CaF_2 transparent ceramics and their corresponding single crystals, the intensity parameters and radiative lifetimes of the ceramics were also compared with the single crystals in the meanwhile.

2. Theory

According to J–O theory, the experimental line strength S_{exp} of the electric-dipole transition from an energy level J to another energy level J' is calculated using the following equation:

$$S_{exp}(J \to J') = \frac{3ch\,(2J+1)}{8\pi^3 e^2 N_0} \frac{9n}{(n^2+2)^2} \frac{2.3}{\bar{\lambda} l} \int_{J\to J'} OD(\lambda) d\lambda \quad (1)$$

where J and J' are the total angular momentum quantum numbers of the initial and final states, c is the velocity of light, h the Planck's constant, e is the electron charge, N_0 is the number of RE^{3+} ions per unit volume, n is the refractive index, $\bar{\lambda}$ is the mean wavelength of the transition band.

The experimental line strengths given above are least-squares fitted to the theoretical line strengths S_{theor}. Then by solving a series of equations, the hosts dependent J–O intensity parameters Ω_2, Ω_4 and Ω_6 can be calculated. The theoretical line strengths S_{theor} are given by Judd and Ofelt in the relation :

$$S_{theor}(J \to J') = \sum_{t=2,4,6} \Omega_t \,|\langle (S,\ L)J \| U^{(t)} \| (S',\ L')J' \rangle|^2 = S_{exp}(J \to J') \quad (2)$$

where S, L are the total spin and total orbit quantum numbers, $\langle \| U^{(t)} \| \rangle$ are the doubly reduced unit tensor operators calculated in the intermediate coupling approximation. Values of the $U^{(t)}$ elements, which vary with different RE^{3+} ions and almost remain the same in different hosts, are taken from Ref. [28].

The root mean square deviation (RMS) error, which defines the accuracy of J–O results, is given by:

$$\text{RMS error} = \sqrt{\sum_{J'} \frac{(S_{exp} - S_{theor})^2}{N-3}} \Big/ \sqrt{\sum_{J'} \frac{S_{exp}^2}{N}} \times 100\% \quad (3)$$

where N is the number of the absorption transitions.

With Ω_t (t = 2, 4, 6) determined, the radiative transition rates and branching ratios for $^4F_{3/2} \to {}^4I_J$ (J = 9/2, 11/2, 13/2 and 15/2) transitions of Nd^{3+} can then be calculated. The transition rate is given by:

$$A_{rad}[(S,L)J;(S'L')J'] = \frac{64\pi^4 e^3}{3h(2J+1)\lambda^3} \times \left[\frac{n(n^2+2)^2}{9}\right] \times \sum_{t=2,4,6} \Omega_t \,|\langle (S,\ L)J \| U^{(t)} \| (S',\ L')J' \rangle|^2 \quad (4)$$

The fluorescence branching ratio for a particular terminal J' manifold can then be defined by:

$$\beta(J \to J') = \frac{A(J \to J')}{\sum_{J'} A(J \to J')} \quad (5)$$

where the sum is over all possible terminal manifolds J'. The sum represents the total transition probability for radiative decay from the initial manifold.

The radiative lifetime of a level is related to the total transition probability as:

$$\tau_{rad} = \frac{1}{\sum_{J'} A(J \to J')} \quad (6)$$

3. Experimental

The precursor nanopowders were synthesized via a co-precipitation method [26], and then vacuum hot-pressed to transparent ceramics. Commercially available reagents (produced by Sinopharm Chemical Reagent Co. Ltd, Shanghai, China) of strontium nitrate ($Sr(NO_3)_2$, 99.9%), hydrated calcium nitrate ($Ca(NO_3)_2{\cdot}4H_2O$, 99.9%), hydrated neodymium nitrate ($Nd(NO_3)_3{\cdot}6H_2O$, 99.9%) and hydrated potassium fluoride ($KF{\cdot}2H_2O$, 99.9%) were used as starting reagents. To perform the J–O analysis, the ceramics are required of high transmittance. However, the transmittances of Nd: SrF_2 and Nd: CaF_2 ceramics are decreased with decrease in Nd^{3+} doping concentration. To ensure high optical quality of the ceramics, we choose the Nd^{3+} doping concentration as 5 mol% in this work. The Nd^{3+} doped SrF_2 nanopowder was synthesized from the following steps: the cationic solution (Sr^{2+} and Nd^{3+}) was made by dissolving strontium nitrate and hydrated neodymium nitrate in distilled water with strontium and neodymium total concentration of 1.0 M. The total concentration was determined by the stoichiometric ratio of the molecular formula $Sr_{0.95}Nd_{0.05}F_{2.05}$. The anionic solution ($F^-$) was made by dissolving hydrated potassium fluoride in distilled water with a concentration of 1.0 M. Both cationic and anionic solutions were separately stirred for 5 min. After this procedure, the cationic solution was added dropwise to the anionic solution with magnetically stirred to form Nd: SrF_2 nanoparticles. After 4 h room temperature staying, the mixture aqueous solution was centrifuged at 11,000 rpm for 15 min. Then the $Sr_{0.95}Nd_{0.05}F_{2.05}$ precipitation was scraped off from the centrifuge tube and ultrasonic dispersing washed in distilled water for 10 min. The centrifugation and washing processes were repeated three times. Then the recovered nanoparticles were oven dried at 80 °C for 24 h and crushed in an agate mortar to obtain the final $Sr_{0.95}Nd_{0.05}F_{2.05}$ nanopowder. The $Ca_{0.95}Nd_{0.05}F_{2.05}$ nanopowder was synthesized in the same way, except replacing strontium nitrate with hydrated calcium nitrate as starting reagent.

The obtained precursor nanopowders were filled into a graphite mold with a cavity diameter of 16 mm and sintered in a carbon heated vacuum furnace (Shanghai Chenrong Electrical Furnace Co. Ltd., Shanghai, China) at 800 °C, under an axial pressure of 30 MPa and a vacuum of about 5.0×10^{-3} Pa. The heating rate was 15 °C/min, and the annealing time was 120 min.

Powder X-ray diffraction (XRD) measurements were taken on a D/Max-RB (Rigaku, Japan), with Cu K_α radiation (λ = 1.54056 Å). The field-emission scanning electron microscope (FESEM; ULTRA, PLUS-43-13, Zeiss, Oberkochen, Germany, operated at 5KV) was used to analyze the microstructure of the ceramic samples. The transmittance spectra and absorption spectra in a range of 200–2500 nm were measured from Lambda 750 (PerkinElmer, USA). The Nd^{3+} content determinations of the ceramics were assessed with inductively coupled plasma optical emission spectroscopy (ICP-OES) using Prodigy 7 (Leeman, America) with argon gas pressure of 0.3 MPa, and the actual contents of Nd^{3+} in Nd: SrF_2 ceramic and Nd: CaF_2 ceramic were measured to be 4.69 mol% and 4.74 mol%, respectively. The luminescence spectra and the luminescence decay data of the ceramic samples excited with Xe lamp were obtained from a fluorescence spectrophotometer (FLS920, Edinburgh, UK) using a near-infrared photomultiplier tube (NIR-PMT) detector. All the measurements were performed at room temperature.

4. Results and discussion

4.1. Structure and phase analysis

Pure SrF_2 and CaF_2 are belong to fluorite lattice structure (space

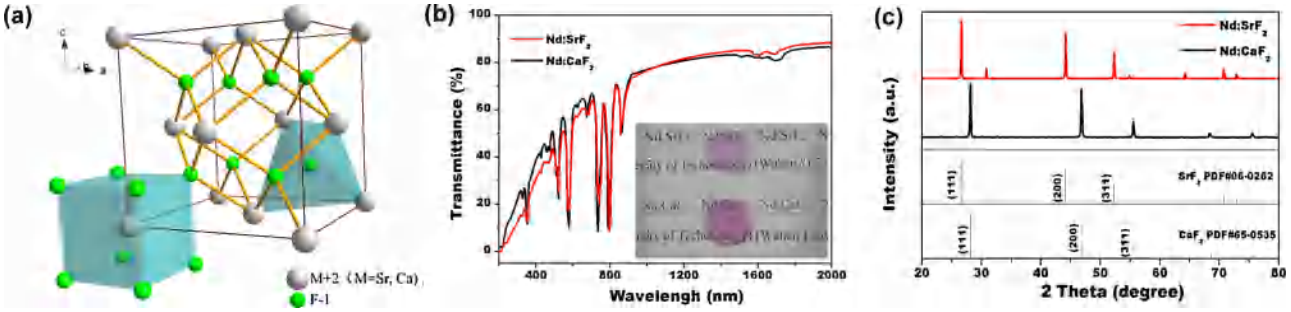

Fig. 1. (a) Fluorite lattice structure, (b) transmittance spectra and (c) X-ray diffraction patterns of Nd: SrF_2 and Nd: CaF_2 transparent ceramics. Inset of Fig. 1b is the appearance of these two ceramics, upper half of the inset is Nd: SrF_2, the other is Nd: CaF_2.

group $Fm\bar{3}m$, Fig. 1a). In this kind of structure, Sr^{2+}/Ca^{2+} ions are situated at corners of the cubic lattice and centers of the cubic face (lattice positions 4a), while the F^- ions are located in the tetrahedral holes (lattice positions 8c). This kind of structure has an important feature that the Sr^{2+}/Ca^{2+} ions occupy every other cubic sublattice center which formed by eight F^-, the other center is empty. The empty sites are known as the interstitial sites and can be occupied by charge compensation F^- ions when Sr^{2+}/Ca^{2+} ions were replaced by Nd^{3+} ions. Fig. 1b shows the transmittance spectra of Nd^{3+} doped SrF_2 and CaF_2 transparent ceramics, the inset displays their appearance with diameter of 16 mm and thickness of 2.0 mm. As can be seen, the ceramics are transparent by naked eye and the letters can be recognized, the transmittance around 1.0 μm are above 75%. Fig. 1c presents the X-ray diffraction patterns of these two ceramics. As shown in the XRD diffractograms, the prominent peaks of Nd: SrF_2 and Nd: CaF_2 ceramics are well corresponding to the cubic fluorite-type SrF_2 (JCPDS file No. 06-0262) and CaF_2 (JCPDS file No. 65-0535) structures, respectively, indicating pure phase of the ceramics.

4.2. Absorption properties and J–O analysis

The room temperature absorption spectra of these two transparent ceramics recorded in wavelength range of 300–1000 nm were shown in Fig. 2a. A series of absorption peaks marked in the figure are derived from the 4f → 4f transitions of Nd^{3+}. The Stark structures of most peaks are poorly resolved due to inhomogeneous broadening of these bands. It can be inferred from Fig. 2a that all the observed peak positions of these two different samples are approximately at the same wavelength, but their shapes are qualitatively different. In particular, the spectrum of Nd: CaF_2 ceramic shows most intensive absorption feature at 736 nm and an energy level splitting at 796 nm (consists of two features at 796 nm and 792 nm). On the contrary, the Nd: SrF_2 sample is characterized by prominent sharp feature at 798 nm and an energy level splitting at 736 nm (consists of two features at 732 nm and 742 nm). Similar phenomena were observed in Nd^{3+} doped phosphate and sodium borate glasses [17,18]. When the concentration of sodium was changed, the relative intensity ratio between the absorption peaks and the band shape were also varied. The authors attributed this change to different Nd^{3+} environment since the crystal field asymmetry varied with different glass composition. Thus, the situation in present work provides an evidence of different crystal field environment of Nd^{3+} ions in SrF_2 and CaF_2 transparent ceramics and due to which, it can be assumed that the luminescence performances of Nd^{3+} in these two hosts are different.

Fig. 2b displays the absorption cross-section curves of these two transparent ceramics, the absorption cross-sections were calculated using the formula:

$$\sigma_{abs} = \frac{2.303OD(\lambda)}{N_0 l} \quad (7)$$

where $OD(\lambda)$ is the optical density at wavelength λ, directly measured by the absorption spectrum. N_0 is the number of Nd^{3+} ions per unit volume, here are 9.61×10^{20} ions/cm^3 for Nd: SrF_2 and 1.15×10^{21} ions/cm^3 for Nd: CaF_2, l is the thickness of the ceramic sample, here are 0.2 cm for both Nd: SrF_2 and Nd: CaF_2. The calculations showed almost no difference in maximum absorption cross-section as they were 1.01×10^{-20} cm^2 for Nd: SrF_2 transparent ceramic and 1.02×10^{-20} cm^2 for Nd: CaF_2 sample. The obtained peak absorption cross-sections of these two transparent ceramics are little higher than their corresponding single crystals (0.79×10^{-20} cm^2 for Nd: SrF_2 single crystal [2] and 0.75×10^{-20} cm^2 for Nd: CaF_2 single crystal [19]), however, it should be mentioned that the conclusion that the Nd: SrF_2 and Nd: CaF_2 transparent ceramics have better absorption properties than their corresponding single crystals should not be made since the differences are very small. Besides of calculation error, one can not be ignored is the absorption caused by residual pores and grain boundaries in ceramics (see further), which may enlarge the absorbance in absorption spectra and contribute to larger absorption cross-sections.

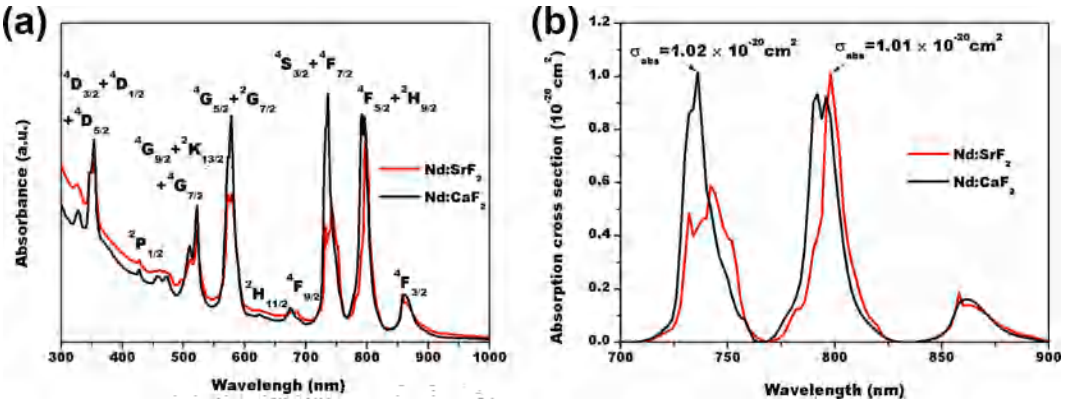

Fig. 2. (a) Room temperature absorption spectra and (b) measured absorption cross-section curves of Nd: SrF_2 and Nd: CaF_2 transparent ceramics.

Table 1
Experimental and theoretical line strengths (10^{-20} cm^2) for Nd^{3+} doped SrF_2 and CaF_2 transparent ceramics.

Transitions (from $^4I_{9/2}$)	SrF_2			CaF_2		
	$\bar{\lambda}$ (nm)	S_{exp}	S_{theor}	$\bar{\lambda}$ (nm)	S_{exp}	S_{theor}
$^4F_{3/2}$	869.6	0.40	0.54	867.6	0.38	0.58
$^4F_{5/2}$ + $^2H_{9/2}$	798.8	1.56	1.54	795.3	1.76	1.78
$^4S_{3/2}$ + $^4F_{7/2}$	741.6	1.44	1.48	737.5	1.74	1.77
$^4F_{9/2}$	680.1	0.09	0.11	677.4	1.18	1.24
$^2H_{11/2}$	627.8	0.01	0.03	624.4	0.01	0.03
$^4G_{5/2}$ + $^2G_{7/2}$	577.6	1.68	1.69	576.8	2.02	2.04
$^2K_{13/2}$ + $^4G_{7/2}$ + $^4G_{9/2}$	516.9	0.85	0.70	516.0	1.08	0.79
RMS (10^{-20} cm^2)	0.11			0.18		
RMS error	9.85%			14.0%		

To further investigate the optical properties, J–O theory was taken as a tool. In the J–O treatment, the more transition bands are integrated, the more accurate the results are. However, with respect to the uncertainty deviation arising from the baseline subtraction, only seven absorption bands located in 500–1000 nm wavelength region were picked to proceed the baseline subtraction and peaks integration processes. The transition band overlapped from two or more absorption manifolds is considered as one with its matrix element taken to be the sum of the corresponding squared matrix elements. Some of the results from J–O theory were shown in Table 1. The RMS errors were measured to be 9.85% and 14.0% for Nd: SrF_2 and Nd: CaF_2 transparent ceramics, respectively. Generally, the computed J–O results are considered credible when the RMS error is in range of 5–25%. Therefore, they can be well applied to further analysis.

It can be seen in Table 1 that, as a continuous trend of band intensities, mostly the line strengths of Nd: SrF_2 transparent ceramic lie on the lower side. In Ref. [2], Payne attributed the larger radiative lifetime of Nd: SrF_2 single crystal (compared with Nd: CaF_2 single crystal) to larger lattice constant, because it led the interstitial charge compensating fluoride (F_i^-) to be slightly farther from Nd^{3+}, and therefore, the F_i^- species were less effective in inducing oscillator strength into the 4f → 4f transitions in Nd: SrF_2 single crystal. As a result, the transition rate is smaller in Nd: SrF_2 single crystal and due to negative correlation between transition rate and radiative lifetime (eq. (6)), the radiative lifetime is larger in Nd: SrF_2 single crystal. In this work, the obtained line strength data agrees well with this assumption.

As the experimental line strengths were determined, the intensity parameters Ω_t (t = 2, 4, 6) were then computed by deriving a set of equations from eq. (2). The results were gathered in Table 2. The intensity parameters of Nd^{3+} doped SrF_2 and CaF_2 single crystals reported in early literatures were also listed for a comparison. Generally, among the intensity parameters, Ω_2 reveals the asymmetry of crystal field and the covalency of the ligand bond, while Ω_4 and Ω_6 indicate the rigidity of the host matrix. The intensity parameters of ceramics were found comparable with those of single crystals. It can be explicitly seen in Table 2 that Ω_2 values of both SrF_2 transparent ceramic and single crystal are smaller than the CaF_2 corresponding hosts, indicating Nd: CaF_2 hosts have more increased crystal field asymmetry of Nd^{3+} environment and higher degree of covalent bonding between Nd^{3+} and the associated ligand. This result is in good agreement with the following two facts that: 1) Concentration quenching occurs at a lower Nd^{3+} content in CaF_2 [2], which means Nd^{3+} has stronger propensity to cluster in CaF_2. The clustering of Nd^{3+} in turn increases the crystal field asymmetry of Nd^{3+} environment. 2) Ca has higher electronegativity than Sr, which leads the bonding in CaF_2 system to be more covalent (Table 3).

Table 2
Intensity parameters for several Nd^{3+} doped materials.

Nd^{3+} doped materials	Judd-Ofelt parameters ($\times 10^{-20}$ cm^2)		
	Ω_2	Ω_4	Ω_6
SrF_2 transparent ceramic	0.47	1.84	2.11
CaF_2 transparent ceramic	0.74	1.93	2.54
SrF_2 single crystal (Ref [2].)	0.24	1.24	1.72
CaF_2 single crystal (Ref [19].)	0.31	0.51	1.24

Table 3
Estimated ionic character for Sr-F and Ca-F bonds (based on Pauling electronegativity).

Bond	Electronegativity difference (Δ_{en})	Estimated ionic character[a]
Sr-F	3.03[b]	89.93%
Ca-F	2.98[b]	89.14%

[a] $= [1\text{-exp}(-(\Delta_{en}^2/4)] \times 100\%$.
[b] electronegativity, Sr is 0.95, Ca is 1.00, F is 3.98.

Interestingly, in Table 2, the Ω_4 value of Nd: SrF_2 transparent ceramic is 1.84×10^{-20} cm^2 which is closed to the Ω_6 value of 2.11×10^{-20} cm^2. In early literature [17], it was found that the Nd^{3+} doped glasses showed larger branching ratio of $^4F_{3/2} \rightarrow {}^4I_{9/2}$ transition ($\beta_{9/2}$) when the value of Ω_4/Ω_6 was increased. The same relationship between Ω_4/Ω_6 and $\beta_{9/2}$ were also reported in literatures [18,29]. It thus can be predicted that, compared with Nd: CaF_2 transparent ceramic, the closer approximation between Ω_4 and Ω_6 in Nd: SrF_2 sample indicates a stronger emission of $^4F_{3/2} \rightarrow {}^4I_{9/2}$ transition. This prediction is further confirmed by emission spectra.

By using the obtained intensity parameters, other radiative parameters such as spontaneous emission transition rates A and branching ratios β were computed, the results were listed in Table 4. The radiative lifetimes, calculated from inverse of the sum of each radiative transition rate, were found to be 1058 μs and 995 μs for Nd: SrF_2 and Nd: CaF_2 transparent ceramics, respectively. These values are little smaller than the corresponding single crystals (1410 μs for Nd: SrF_2 single crystal [2] and 1295 μs for Nd: CaF_2 single crystal [19]). As mentioned above, in addition to the calculation error, the grain boundary scattering and residual pores quenching in ceramics may also be associated with their smaller radiative lifetimes. To have a better understanding of this hypothesis, FESEM measurements of these samples were made. Fig. 3a and 3b are FESEM images showing the fracture surfaces of these two transparent ceramic samples. As is seen, the grain size of both ceramics has a wide distribution for it ranges from about 100 nm to 1000 nm. The fracture models illustrated in the FESEM figures consist of transgranular and intergranular. The residual pores within the microstructure are also clearly observed in the photographs. For comparison, Fig. 3c shows the fracture surface of Nd: SrF_2 single crystal. It can be seen that there is no grain boundary or residual pore in the single crystal. As is known, the residual pores and grain boundaries are two main scattering sources of polycrystalline transparent ceramics [30]. This implies that, compared with analogous single crystals, the absorptions in Nd: SrF_2 and Nd: CaF_2 transparent ceramics are caused not only by electron transitions in Nd^{3+} 4f shell, but also more or less by the residual pores and grain boundaries. Consequently, the values of

Table 4
Measured radiative properties from $^4F_{3/2}$ level of Nd^{3+} in SrF_2 and CaF_2 transparent ceramics.

Transitions	SrF_2		CaF_2	
	A (s^{-1})	β	A (s^{-1})	β
$^4F_{3/2} \rightarrow {}^4I_{15/2}$	4.57	0.005	5.43	0.005
$^4F_{3/2} \rightarrow {}^4I_{13/2}$	92.11	0.097	108.81	0.108
$^4F_{3/2} \rightarrow {}^4I_{11/2}$	460.03	0.487	517.97	0.516
$^4F_{3/2} \rightarrow {}^4I_{9/2}$	388.14	0.411	372.40	0.371
τ_{rad} ($^4F_{3/2}$)	1058 μs		995 μs	

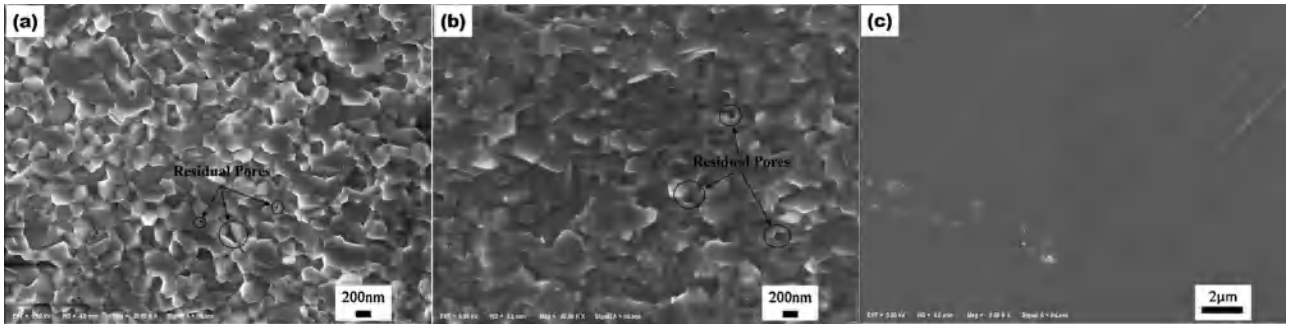

Fig. 3. FESEM images of the Nd^{3+} doped (a) SrF_2 and (b) CaF_2 transparent ceramics, (c) is the FESEM image of Nd^{3+} doped SrF_2 single crystal.

line strengths are larger in the ceramic hosts. From eq. (4) and eq. (6), the radiative lifetimes are thus slightly lower than the analogous single crystals.

On the other hand, the radiative lifetime of Nd: SrF_2 transparent ceramic is larger than Nd: CaF_2 transparent ceramic. This is consistent with the result that the Nd: SrF_2 single crystal has larger radiative lifetime than Nd: CaF_2 single crystal. The comparison of radiative lifetimes indicates Nd^{3+} is easier to realize population inversion in SrF_2 hosts than in CaF_2 hosts.

4.3. Luminescence properties

The room temperature near infrared (NIR) luminescence spectra of these two transparent ceramics recorded in the wavelength range of 830–1450 nm were shown in Fig. 4. As is seen in the spectra, the fluorescence bands located in ranges of 830–950 nm, 1000–1150 nm and 1300–1400 nm are related to transitions of $^4F_{3/2} \rightarrow {}^4I_{9/2}$, $^4F_{3/2} \rightarrow {}^4I_{11/2}$ and $^4F_{3/2} \rightarrow {}^4I_{13/2}$, respectively. For Nd: SrF_2 sample, the $^4F_{3/2} \rightarrow {}^4I_{9/2}$ transition is characterized by obvious broad bimodal and over-estimated band area, revealing extensive Stark splitting of the energy levels and anomalously large value of $\beta_{9/2}$. This is continuous with J–O prediction. The $^4F_{3/2} \rightarrow {}^4I_{11/2}$ transition, which is of interest for solid laser amplifier actions, shows only one apparent sharp peak centered at wavelength of 1053.5 nm with an effective bandwidth ($\Delta\lambda_{eff}$) of 34.8 nm. Generally, owing to electric dipole interaction, the $^4F_{3/2}$ and $^4I_{11/2}$ energy levels will split into two and six sublevels, respectively [31]. Which means, there should be at most twelve pairs of transitions (peaks) in the $^4F_{3/2} \rightarrow {}^4I_{11/2}$ transition band. With this in mind, the luminescence spectrum thus indicates great decrease in variety and quantity of Nd^{3+} luminescence centers. By comparing the radiative lifetimes and emission lifetimes (described further), it was found that

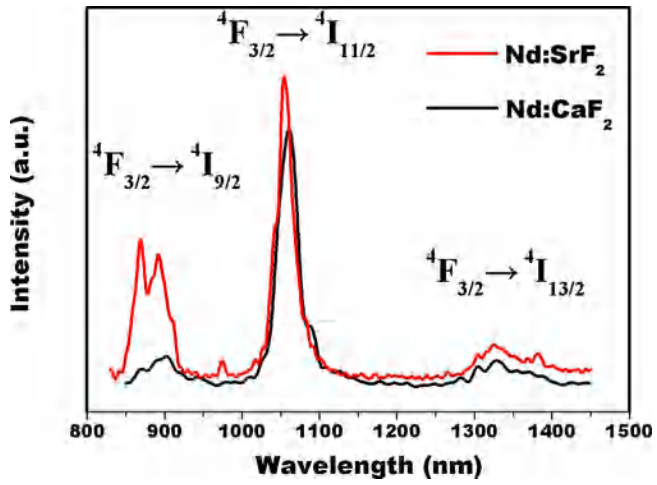

Fig. 4. Room temperature NIR luminescence spectra of Nd: SrF_2 and Nd: CaF_2 transparent ceramics.

concentration quenching occurs in these two samples and therefore, the decreases in variety and quantity of Nd^{3+} luminescence centers can be attributed to this non-radiative process.

In comparison with Nd: SrF_2, the Nd: CaF_2 ceramic presents a much weaker emission of $^4F_{3/2} \rightarrow {}^4I_{9/2}$ transition, and a slightly weaker $^4F_{3/2} \rightarrow {}^4I_{11/2}$ emission centered at 1061 nm with a $\Delta\lambda_{eff}$ of 33.4 nm. The main reason for different features of $^4F_{3/2} \rightarrow {}^4I_{11/2}$ emission between these two samples is lied on more ionic the Nd^{3+}-ligand bonding in SrF_2. Due to nephelauxetic effect, the more ionic the Nd^{3+}-ligand bonding, the stronger electron-electron interactions and hence the higher transition energy. As a result, the peak position shifts to lower wavelength and the emission is more intensive [32–34].

Room temperature luminescence decay curves of the $^4F_{3/2} \rightarrow {}^4I_{11/2}$ emission of Nd: SrF_2 and Nd: CaF_2 transparent ceramics were shown in Fig. 5a and 5b, respectively. As is seen in the figures, both the decay plots can be well fitted by single exponential function. The emission lifetimes τ_{em} of $^4F_{3/2}$ level are measured to be 16.4 μs for Nd: SrF_2 and 9.5 μs for Nd: CaF_2. Although they are much shorter than the radiative lifetimes obtained from J–O theory, but it still follows the trend of $SrF_2 > CaF_2$, confirming the fact that the excited energy level of Nd: SrF_2 has better capability to store energy. The dramatic decreases of measured lifetimes for both Nd: SrF_2 and Nd: CaF_2 indicate 5 mol% Nd^{3+} doping concentration is sufficient high that concentration quenching occurs in the transparent ceramics. The concentration quenching phenomenon, which is quite common among RE^{3+} doped materials, is caused by cross-relaxation (CR) between two nearby Nd^{3+} ions and the critical quenching concentration is varied with different RE^{3+} ions and host materials [2,22,34–38]. Fig. 6 illustrates the mechanism of concentration quenching in Nd: SrF_2. Upper part of Fig. 6 depicts an example of a simple cluster structure that contains two Nd^{3+} ions: two nearest Sr^{2+} ions are replaced by Nd^{3+} ions and two extra F_i^- ions enter into the interstitial sites to balance the charge. When one Nd^{3+} is excited from ground level $^4I_{9/2}$ to the excited level $^4F_{5/2} + {}^2H_{9/2}$ by 798 nm Xe lamp pumping, the ion in $^4F_{5/2} + {}^2H_{9/2}$ level will relax to lower $^4F_{3/2}$ level without radiation, and then this ion transits from $^4F_{3/2}$ level to lower $^4I_{15/2}$ level with a photon emitting out, the other Nd^{3+} absorbs this photon and gets excited from ground $^4I_{9/2}$ level to $^4I_{15/2}$ level without radiation, then this Nd^{3+} ion non-radiatively relaxes from $^4I_{15/2}$ level to ground $^4I_{9/2}$ level (bottom half of Fig. 6). As a result, no emission is gained in these two Nd^{3+} ions. Notably, this energy transfer process can happen easier and faster if the distance between Nd^{3+} ions is smaller [39–41]. In present study, the smaller emission lifetime of Nd: CaF_2 is assigned to closer distance between Nd^{3+} and Nd^{3+} ions (smaller lattice parameter of CaF_2), which leads to higher luminescent quenching rate in Nd: CaF_2.

The data we obtained from J–O theory suggest the Nd: SrF_2 transparent ceramic is more suitable for laser storage mediums and laser amplifiers, since it has longer radiative lifetime and more ionic Nd^{3+}-ligands bonding. These advantages make it easier for Nd: SrF_2 to realize population inversion and strong emission. The concentration quenching of these two samples observed in present study will no doubt limit their

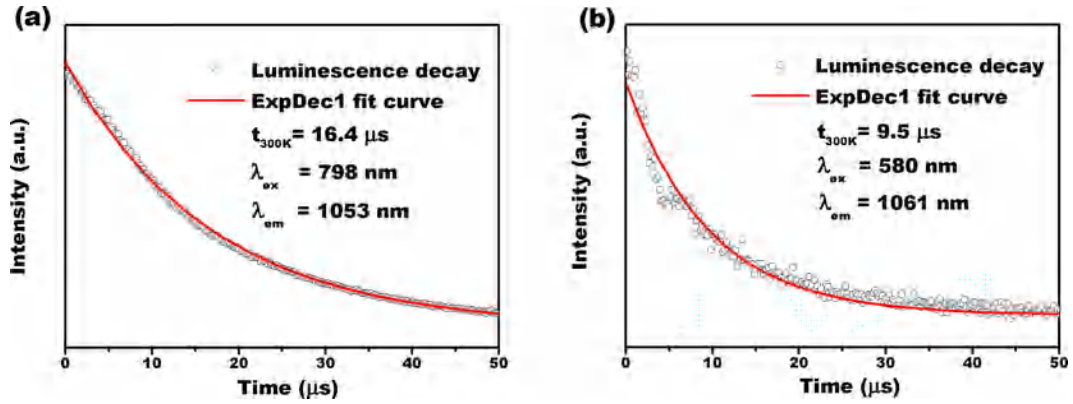

Fig. 5. Luminescence decay curves of (a) Nd: SrF_2 and (b) Nd: CaF_2 transparent ceramics. The fitted lifetime values are displayed in the figure.

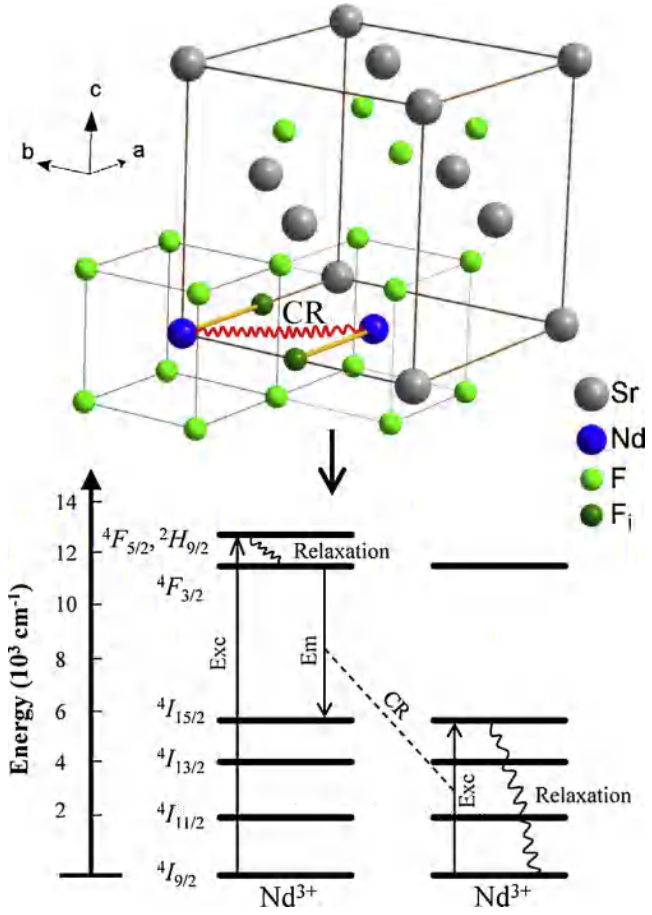

Fig. 6. Example of a simple Nd^{3+} cluster in SrF_2 lattice structure and the cross-relaxation in energy level diagrams between two Nd^{3+} ions.

applications. To solve this matter, further works such as decrease the Nd^{3+} doping content and codope with buffer ions (Y^{3+} or La^{3+}) should be taken into account. Since the Nd: SrF_2 transparent ceramic has a strong emission of $^4F_{3/2} \rightarrow {}^4I_{9/2}$ transition, it is worth mentioning that this situation will be enhanced by decrease of Nd^{3+} doping. Marciniak et al. [41] studied Nd^{3+} doping content as an influence factor on the evolution of $\beta_{9/2}$ and $\beta_{11/2}$ in details and found that, with increase in Nd^{3+} doping, the $\beta_{9/2}$ was decreased and the $\beta_{11/2}$ was increased. This was because the reabsorption process of $^4F_{3/2} \rightarrow {}^4I_{9/2}$ transition became more and more serious with increase in Nd^{3+} doping. It thus can be assumed that, a decrease of Nd^{3+} content, e.g., from 5 mol% to 2 mol%, aiming to weaken concentration quenching and strengthen the luminescence [42], will lead to larger $\beta_{9/2}$ and smaller $\beta_{11/2}$. This feature is of interest for making it possible to achieve effective laser output around 900 nm in Nd: SrF_2 transparent ceramic.

5. Conclusion

Nd^{3+} doped SrF_2 and CaF_2 transparent ceramics were fabricated by a vacuum hot-press sintering method. The ceramics were analyzed by using J–O theory. The results suggested the Nd: SrF_2 transparent ceramic was more suitable for laser applications. Room temperature absorption spectra showed approximately the same wavelength but different relative peak intensity for these two transparent ceramics, indicating different crystal field environment of Nd^{3+} ions in these two ceramics. The obtained maximum absorption cross-sections were quite close. The RMS errors were determined to be 9.85% and 14.0% for Nd: SrF_2 and Nd: CaF_2, respectively, giving validity of the J–O results. Because of larger distance between F_i^- ions and Nd^{3+} ions in Nd: SrF_2 transparent ceramic, the F_i^- ions are less effective in inducing oscillator strength into Nd^{3+} 4f shell, leading the absorption line strength of Nd: SrF_2 to be smaller. The smaller line strength results in a larger radiative lifetime of Nd: SrF_2, by which population inversion of excited levels is favored. The J–O calculation showed Nd: SrF_2 transparent ceramic had smaller Ω_2 and larger Ω_4/Ω_6, indicating more ionic Nd^{3+}-ligand bonding and larger $\beta_{9/2}$ in Nd: SrF_2, respectively. By comparing the experimental lifetimes and radiative lifetimes, it showed that concentration quenching occurred in present samples. Besides, the absorption cross-sections, intensity parameters and radiative lifetimes of Nd: SrF_2 and Nd: CaF_2 transparent ceramics were found comparable with those of Nd: SrF_2 and Nd: CaF_2 single crystals reported in early literatures, suggesting comparable radiative properties between these Nd^{3+} doped alkaline earth fluoride transparent ceramics and single crystals.

Acknowledgements

This work was financially supported by the National Natural Science Foundation of China (No. 51432007).

References

[1] A.A. Kaminskii, V.V. Osico, A.M. Prochoro, Y.K. Voronko, Spectral investigation of the stimulated radiation of Nd^{3+} in CaF_2 - YF_3, Phys. Lett. 22 (1966) 419–421.
[2] S.A. Payne, J.A. Caird, L.L. Chase, L.K. Smith, N.D. Nielsen, W.F. Krupke, Spectroscopy and gain measurements of Nd^{3+} in SrF_2 and other fluorite-structure hosts, J. Opt. Soc. Am. B 8 (1991) 726–740.
[3] T.T. Basiev, V.V. Fedorov, A.Y. Karasik, K.K. Pukhov, Strong coherent interaction of Nd^{3+}-Nd^{3+} pair ions in CaF_2 crystal, J. Lumin. 81 (1999) 189–197.
[4] Z.D. Liu, B.C. Mei, J.H. Song, W.W. Li, Optical characterizations of hot-pressed erbium-doped calcium fluoride transparent ceramic, J. Am. Ceram. Soc. 97 (2014) 2506–2510.
[5] G. Singh, R. Selvamani, V.S. Tiwari, A.K. Karnal, Spectroscopic investigations of

Nd^{3+} doped PLZT ceramics on the basis of Judd-Ofelt theory, J. Lumin. 192 (2017) 1084–1088.
[6] V. Petit, P. Camy, J.-L. Doualan, R. Moncorgé, CW and tunable laser operation of Yb^{3+} in Nd:Yb:CaF_2, Appl. Phys. Lett. 88 (2006) 1–3 05111.
[7] F.K. Ma, D.P. Jiang, L.B. Su, J.Y. Wang, W. Cai, J. Liu, J.G. Zheng, W.G. Zheng, J. Xu, Y. Liu, Spectral properties and highly efficient continuous-wave laser operation in Nd-doped $Sr_{1-x}Y_xF_{2+x}$ crystals, Opt. Lett. 41 (2016) 501–503.
[8] W.W. Li, B.C. Mei, J.H. Song, Nd^{3+}, Y^{3+} codoped SrF_2 laser ceramics, Opt. Mater. 47 (2015) 108–111.
[9] A. Ikesue, Y.L. Aung, Synthesis and performance of advanced ceramic lasers, J. Am. Ceram. Soc. 89 (2006) 1936–1944.
[10] A. Ikesue, T. Kinoshita, K. Yoshida, Fabrication and optical properties of high-performance polycrystalline Nd: YAG ceramics for solid-state lasers, J. Am. Ceram. Soc. 78 (1995) 1033–1040.
[11] A. Lyberis, A.J. Stevenson, A. Suganuma, S. Ricaud, F. Druon, R. Herbst, D. Vivien, P. Gredin, M. Mortier, Mortier, Effect of Yb^{3+} concentration on optical properties of Yb: CaF_2 transparent ceramics, Opt. Mater. 34 (2012) 965–968.
[12] T.T. Basiev, M.E. Doroshenko, P.P. Fedorov, V.A. Konyushkin, S.V. kuznetsov, V.V. Osiko, M.Sh. Akchurin, Efficient laser based on CaF_2-SrF_2-YbF_3 nanoceramics, Opt. Lett. 33 (2008) 521–523.
[13] T.T. Basiev, M.E. Doroshenko, V.A. Konyushkin, V.V. Osiko, SrF_2:Nd^{3+} laser ceramics, Opt. Lett. 35 (2010) 4009–4011.
[14] T.T. Basiev, V.A. Konyushkin, D.V. Konyushkin, M.E. Doroshenko, G. Huber, F. Reichert, N. Hansen, M. Fechner, First ceramic laser in the visible spectral range, Opt. Mater. Exp. 1 (2011) 1511–1514.
[15] B.R. Judd, Optical absorption intensities of rare-earth ions, Phys. Rev. 127 (1962) 750–761.
[16] G.S. Ofelt, Intensities of crystal spectra of rare-earth ions, J. Chem. Phys. 37 (1962) 511–520.
[17] V. Mehta, G. Aka, A.L. Dawar, A. Mansingh, Optical properties and spectroscopic parameters of Nd^{3+}-doped phosphate and borate glasses, Opt. Mater. 12 (1999) 53–63.
[18] R.T. Karunakaran, K. Marimuthu, S. Arumugam, S.S. Babu, S.F. Leon-Luis, C.K. Jayasankar, Structural, optical absorption and luminescence properties of Nd^{3+} ions in NaO-NaF borate glasses, Opt. Lett. 32 (2010) 1035–1041.
[19] Q.G. Wang, L.B. Su, H.J. Li, L.H. Zheng, X. Guo, D.P. Jiang, H.Y. Zhao, J. Xu, W. Ryba-Romanwski, P. Solarz, R. Lisiecki, Optical spectra and excited state relaxation dynamics of Nd^{3+} in CaF_2 single crystal, J. Alloys. Compd. 509 (2011) 8880–8884.
[20] H. Ping, D.Q. Chen, Y.L. Yu, Y.S. Wang, Judd-Ofelt analyses and luminescence of Er^{3+}/Yb^{3+} co-doped transparent glass ceramics containing $NaYF_4$ nanocrystals, J. Alloys. Compd. 490 (2010) 74–77.
[21] C. Sin, T. Aidilibike, W.P. Qin, C.-J. Yu, Mechanism for ultraviolet luminescence of Gd^{3+} ions sensitized by Yb^{3+} clusters in CaF_2:Yb^{3+}, Gd^{3+}, J. Lumin. 194 (2018) 72–74.
[22] G.L. Zhi, J.H. Song, B.C. Mei, W.B. Zhou, Synthesis and characterization of Er^{3+} doped CaF_2 nanoparticles, J. Alloys. Compd. 509 (2011) 9133–9137.
[23] Z.D. Liu, B.C. Mei, J.H. Song, W.W. Li, Fabrication and optical characterizations of Yb, Er codoped CaF_2 transparent ceramic, J. Eur. Ceram. Soc. 34 (2014) 4389–4394.
[24] W.W. Li, B.C. Mei, J.H. Song, Z. Wang, Fabrication and optical properties of highly transparent SrF_2 ceramic, Mater. Lett. 159 (2015) 210–212.
[25] Z.D. Liu, B.C. Mei, J.H. Song, D. Yuan, Z. Wang, Microstructure and optical properties of hot-pressed Er:CaF_2 transparent ceramics, J. Alloys. Compd. 646 (2015) 760–765.
[26] Z.W. Zhou, W.W. Li, J.H. Song, G.Q. Yi, B.C. Mei, L.B. Su, Synthesis and characterization of Nd^{3+} doped SrF_2 nanoparticles prepared by precipitation method, Ceram. Int. 44 (2018) 4344–4350.
[27] Y.G. Jiang, B.X. Jiang, Q.H. Zhu, N. Jiang, P.D. Zhang, S.L. Chen, X. Hu, G. Zhang, J.T. Fan, L.B. Su, J. Li, L. Zhang, Effects of deformation rate on properties of Nd,Y-codoped CaF_2 transparent ceramics, J. Eur. Ceram. Soc. 38 (2018) 2404–2409.
[28] A.A. Kaminskii, G. Boulon, M. Buoncristiani, B.D. Bartolo, A. Kornienko, V. Mironov, Spectroscopy of a new laser garnet $Lu_3Sc_2Ga_3O_{12}$:Nd^{3+}. Intensity luminescence characteristics, stimulated emission, and full set of squared reduced matrix elements $|\langle\|U(t)\|\rangle|2$ for Nd^{3+} ions, Phys. Stat. Sol. A 141 (1994) 471–494.
[29] M. Ajroud, M. Haouari, H.B. Ouada, H. Maaref, A. Brenier, C. Garapon, Investigation of the spectroscopic properties of Nd^{3+}-doped phosphate glasses, J. Phys.: Condens. Mater. 12 (2000) 3181–3193.
[30] S.E. Hatch, W.F. Parsons, R.J. Weagley, Hot-pressed polycrystalline CaF_2:Dy^{2+} laser, Appl. Phys. Lett. 8 (1964) 153–154.
[31] T.P.J. Han, G.D. Jones, R.W.G. Syme, Site-selective spectroscopy of Nd^{3+} centers in CaF_2:Nd^{3+} and SrF_2:Nd^{3+}, Phys. Rev. B 47 (1993) 706–723.
[32] M.J. Weber, D.C. Ziegler, A. Angell, Tailoring stimulated emission cross sections of Nd^{3+} laser glass: Observation of large cross section for $BiCl_3$ glasses, J. Appl. Phys. 53 (1982) 4344–4350.
[33] A. Tesar, J. Campbell, M. Webber, C. Weinzapfel, Y. Lin, H. Meissner, H. Toratani, Optical properties and laser parameters of Nd^3-doped fluoride glasses, Opt. Mater. 1 (1992) 217–234.
[34] H. Rinnert, P. Miska, M. Vergnat, G. Schmerber, S. Colis, A. Dinia, D. Muller, G. Ferblantier, A. Slaoui, Photoluminescence of Nd-doped SnO_2 thin films, Appl. Phys. Lett. 100 (2012) 1–3 101908.
[35] C.X. Li, C.M. Zhang, Z.Y. Hou, L.L. Wang, Z.W. Quan, H.Z. Lian, J. Lin, β-$NaYF_4$ and β-$NaYF_4$:Eu^{3+} microstructures: morphology control and tunable luminescence properties, J. Phys. Chem. C 113 (2009) 2332–2339.
[36] M. Misiak, K. Prorok, B. Cichy, A. Bednarkiewicz, W. Strek, Thulium concentration quenching in the up-converting α-Tm^{3+}/Yb^{3+} $NaYF_4$ colloidal nanocrystals, Opt. Mater. 35 (2013) 1124–1128.
[37] Q. Wang, J.B. Qiu, Z.G. Song, Z.W. Yang, Z.Y. Yin, D.C. Zhou, Optical properties of Ce^{3+}-Nd^{3+} co-doped YAG nanoparticles for visual and near-infrared biological imaging, Spectrochim Acta A 149 (2015) 898–903.
[38] R.J. Wiglusz, L. Marciniak, R. Pazik, W. Strek, Structural and spectroscopic characterization of Nd^{3+}-doped YVO_4 yttrium orthovanadate nanocrystallites, Cryst. Growth Des. 14 (2014) 5512–5520.
[39] Y.V. Orlovskii, T.T. Basiev, S.A. Abalakin, I.N. Vorob'ev, O.K. Alimov, A.G. Papashvili, K.K. Pukhov, Fluorescence quenching of the Nd^{3+} ions in different optical centers in fluorite-type crystals, J. Lumin. 76–77 (1998) 371–376.
[40] Y.V. Orlovskii, V.V. Fedorov, T.T. Basiev, M. Altwein, B. Leu, J. Heber, S. Mirov, Nonradiative relaxation and inhomogeneous splitting of aggregated optical centers in the Nd^{3+}-doped CaF_2 and SrF_2 crystals (FLN and decay study), J. Lumin. 83–84 (1999) 361–366.
[41] L. Marciniak, W. Strek, Y. Guyot, D. Hreniak, G. Boulon, Synthesis and Nd^{3+} luminescence properties of $ALa_{1-x}Nd_xP_4O_{12}$ (A = Li, Na, K, Rb) tetraphosphate nanocrystals, J. Phys. Chem. C 119 (2015) 5160–5167.
[42] S.N. Rasool, T. Sasikala, B.A. Mohan, M.L. Rama, C.K. Jayasankar, Optical spectroscopy, 1.06 μm emission properties of Nd3 + -doped phosphate based glasses, Spectrochim Acta A 180 (2017) 193–197.